Spectroscopy of Cr^{3+} and Cr^{4+} ions in forsterite

Weiyi Jia, Huimin Liu, S. Jaffe, and W. M. Yen
Department of Physics and Astronomy, University of Georgia, Athens, Georgia 30602

B. Denker
Institute of General Physics, Academy of Sciences of the Union of Soviet Socialist Republics, Lenin Prospect 53, 117924 Moscow, Russia

(Received 22 June 1990; revised manuscript received 4 October 1990)

Fluorescence and site-selective excitation spectra of chromium-activated forsterite at 10 K are reported. It is found that a high-field Cr^{3+} site in inversion symmetry emits sharp R_1 line fluorescence, while a low field Cr^{3+} site in mirror symmetry produces $^4T_2$ broadband emission. The dominant absorption in the visible is shown to be the $^3A_2 \rightarrow {}^3T_1(^3F)$ transitions of Cr^{4+} in tetrahedral sites. In the near-infrared region, three sharp lines from Cr^{4+} were observed and are assigned to the transition from the $^3A_1(^3T_2)$ spin triplet to the $^3A_2$ ground state. The energy-level splittings of Cr^{4+} due to an orthorhombic-distorted field with spin-orbit coupling are discussed.

I. INTRODUCTION

There has been considerable research interest in tunable solid-state laser materials since the advent of the first broadly tunable, room-temperature alexandrite laser.[1] Similar lasers have been demonstrated for Cr^{3+} in other crystal hosts, for example, gadolinium scandium gallium garnet.[2] New lasing ions, such as Ti^{3+}, have also been employed.[3]

Recently, Petricevic *et al.*[4,5] added a new lasing media, Cr^{4+} -doped forsterite to the family of tunable solid-state laser materials, and expanded the tunable spectral range to the near infrared (NIR) spanning the 1.167- to 1.345-μm range. Such a forsterite laser was also reported by Verdun *et al.*[6]

Cr^{4+} ions possess a $3d^2$ configuration, and are the simplest non-Kramer ions among transition elements. Other examples of $3d^2$ ions, such as V^{3+} and Ti^{2+}, have been extensively studied,[7,8] and fluorescent emission in the IR from these ions have been observed. However, no lasing action from these two ions has been reported. In this sense, Cr^{+4} is unique and thus of interest.

Since Cr^{4+} and Cr^{3+} coexist in forsterite, it is easy to misassign the spectra. In fact, Petricevic *et al.* first ascribed the lasing transition to Cr^{3+},[5] only later they did assign it to Cr^{4+}.[6] Moncorge *et al.* have reported the spectroscopic properties of forsterite and identified the spectra of Cr^{4+}.[6,9]

In this work a more detailed spectroscopic study on Cr activated Mg_2 SiO_4 was carried out. The corresponding electronic transitions from both Cr^{3+} and Cr^{4+} were identified and are presented below.

II. EXPERIMENTAL DETAILS

Two types of samples were used in this experiment: bulk crystals and single crystal fibers. The bulk sample contained 0.2 at. % Cr and had dimension $5\times3\times2.5$ mm^3. The fiber samples were grown in air by the laser-heated pedestal method in our laboratory.[10] The content of Cr^{4+} in the fibers was found to be dependent on the growth atmosphere, increasing when pure O_2 is employed.[10] The fibers used in this study had diameters of $\sim$0.7 mm. The fibers were aligned along the crystallographic axis.

The samples were mounted onto the cooling finger of a closed-cycle refrigerator capable of reaching temperatures down to 10 K. The measurements in the NIR were done with a 0.85-m single-grating SPEX spectrometer and Varian VMP 159A or a Ge photodiode coupled to lock-in detection. In the visible region measurements were performed with a double-grating SPEX spectrometer. A 1-KW tungsten filament lamp and a quarter meter monochrometer was used as a light source in the excitation spectrum measurements. For absorption measurement, a 40-W tungsten lamp was used. Fluorescence spectra were obtained with the 514.5- and 488-nm Ar^+ laser lines and with a dye laser.

III. EXPERIMENTAL RESULTS

A. Crystal structure

In order to understand the experimental data, a short introduction of the crystal structure of Mg_2SiO_4 is given here.

Mg_2SiO_4 (α-Mg_2SiO_4), or forsterite, is a member of the olivine family. It has an orthorhombic structure with space group P_{bnm} and contains four formula units per unit cell.[11] The unit cell dimensions are $a=4.76$ Å, $b=10.22$ Å, $c=5.99$ Å. In the hexagonal close-packed array of oxygen atoms, one-half of the available octahedral voids are occupied by Mg atoms, and one-eighth of the available tetrahedral voids occupied by Si atoms. The Mg ions are in two crystallographically distinct positions, 4*a* and 4*c*, which have inversion ($\bar{1}$) and mirror (*m*) point symmetries, designated as *M*1 and *M*2, respectively The position of Si ions, 4*c*, has the point symmetry of (m). All the polyhedra are extremely distorted.[11]

The occupied octahedra form serrated chains parallel

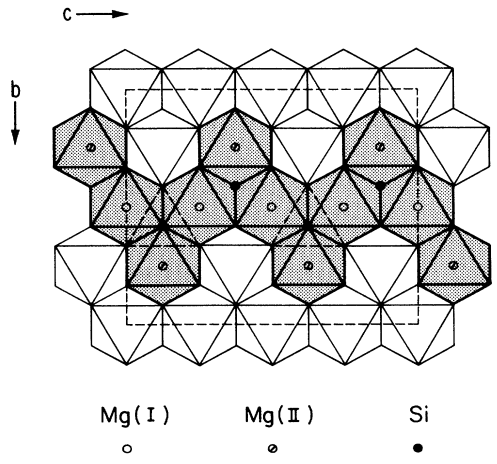

FIG. 1. A serrated chain of the occupied octahedral and tetrahedral sites (shaded) in the crystal structure of forsterite [after Birle *et al.* (Ref. 11)].

to the $c(z)$ axis (Fig. 1).[11] The $M1$ octahedra serve as the spine with the $M2$ octahedra as the teeth distributed alternatively along the chain in the yz plane. Si tetrahedra connect between these two type of octahedra. Large spectroscopic anisotropy can be expected for such a structure; in fact, Cr-doped forsterite exhibits dichroic properties. To the eyes it appears greenish, bluish and reddish when looking through the a, b, and c axis, respectively.

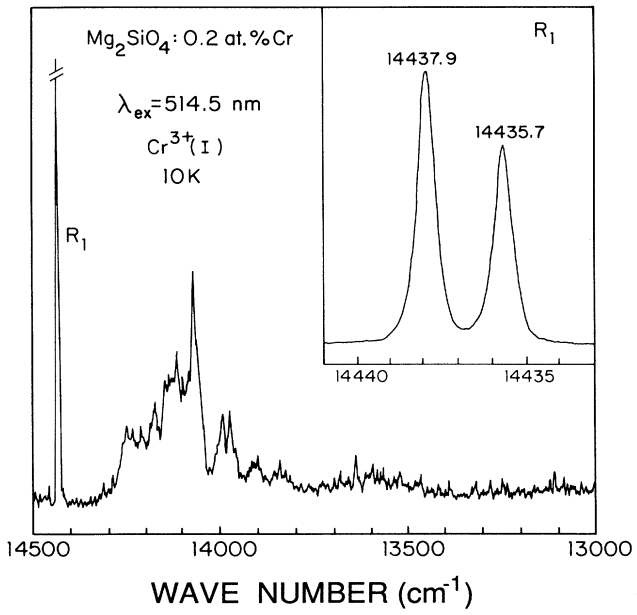

FIG. 2. R_1-line fluorescence and the corresponding phonon sideband from Cr^{3+}(I) high field site in forsterite fibers at 10 K. Double lines are due to spin-orbit splitting of the $^4A_2$ ground state.

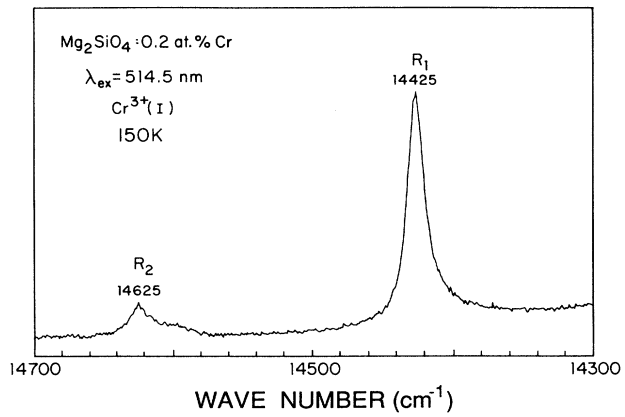

FIG. 3. R_2 emission from thermal population of $2\bar{A}$ sublevel of the ^2E state of Cr^{3+}(I) at 150 K. The splitting of the ^2E state is 200 cm^{-1}.

B. Fluorescence

Fluorescence was investigated over the visible and NIR region. The results for bulk and fiber samples are the same, so that results apply to both types of samples. At 10 K strong and sharp fluorescence spectrum is observed in the visible, as shown in Fig. 2. The peak consists of a doublet peaking at 14437.9 cm^{-1} (692.62 nm) and 14435.7 cm^{-1} (692.73 nm) (see the inset) with linewidths of 0.6 cm^{-1}. We assign this structure to the ^2E level of Cr^{3+}(I) in the inversion- symmetric octahedron [Mg (I) site]. This corresponds to the R_1 line transition; the doublet structure arises from the spin-orbit splitting of the $^4A_2$ ground state. The corresponding R_2 line of Cr^{3+}(I) is not observed at 10 K, but appears at higher temperature (see Fig. 3). This thermal behavior allows us to con-

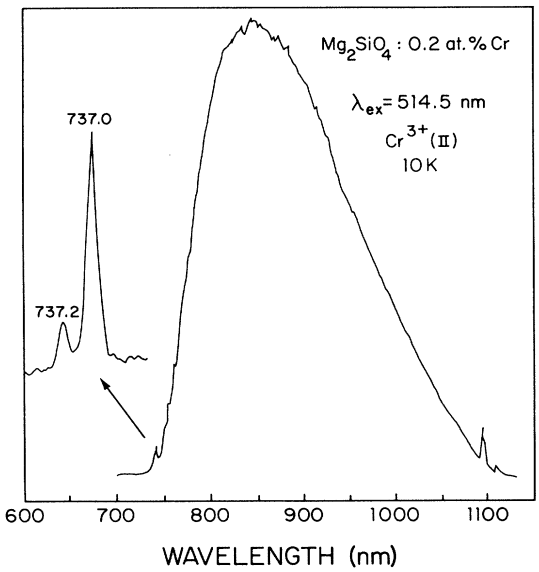

FIG. 4. Broad-band emission ($^4T_2 \rightarrow {}^4A_2$) from Cr^{3+}(II) low field site. The weak peaks at the high energy side are the $^4T_2$ zero-phonon lines.

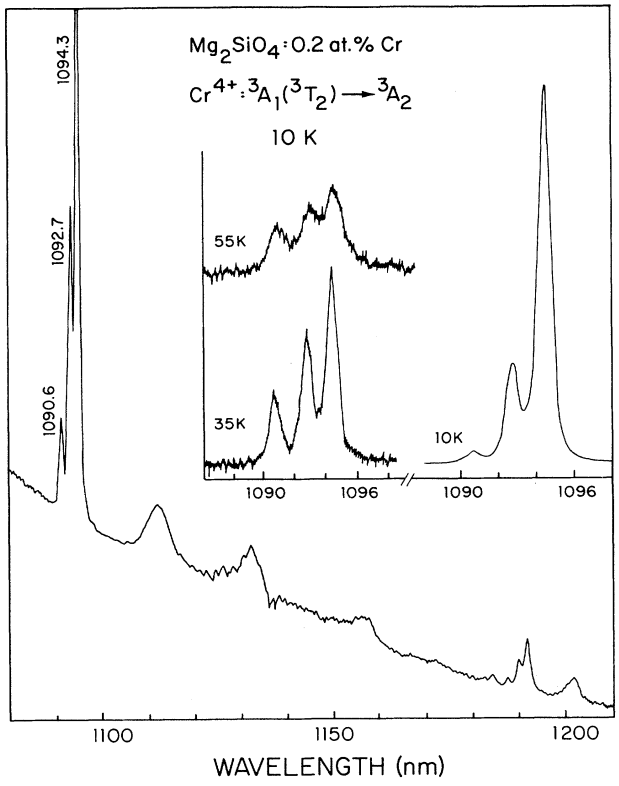

FIG. 5. The spectra from $^3A_1(^3T_2) \rightarrow {}^3A_2$ transition of Cr^{4+} ions in tetrahedral sites in forsterite. The three sharp lines are from the spin-orbit splitting of $^3A_1(^3T_2)$. The peaks at the long wavelength side are the corresponding phonon satellites. The temperature dependence of the relative intensities is shown in the inset.

clude that the ^2E experiences a large uniaxial splitting ($\Delta = 200$ cm^{-1}). The lifetime of the R_1 line is 6.5 ms at 10 K and drops down to 240 μs at room temperature. The broad structural features below the R_1 line have the same lifetime and are of vibronic origin.

In addition, at 10 K a broad emission band peaking at 866 nm (11 600 cm^{-1}) is observed as shown in Fig. 4. It originates from the $^4T_2 \rightarrow {}^4A_2$ transition of Cr^{3+}(II) ions at the octahedron of mirror symmetry [Mg(II) site]. The weak sharp doublet, peaking at 13 564 cm^{-1} (737.25 nm) and 13 568 cm^{-1} (737.03 nm), are the zero-phonon origins of $^4T_2$. The lifetime of the $^4T_2$ emission does not change significantly. It was measured to be 17 μs at 10 K and 12 μs at room temperature. In contrast to Cr^{3+}(I), Cr^{3+} (II) is in a low field site, in which the ^2E state of the Cr^{3+} is above the $^4T_2$ state. This is because the Mg(II) octahedron is large than the Mg(I) octahedron, with the average O—Mg bond length of the former being 2.135 Å, compared to 2.103 Å for the latter.[11]

It should be mentioned that the substitution of Mg^{2+} by Cr^{3+} requires charge compensation,and interstitial oxygen should appear in the crystals. The defects are expected to change the site symmetry and the strength of crystal field of the site. However, no additional emission peaks from such inequivalent centers in quality samples were observed. Rager *et al.*[12] have shown from their EPR results that the interstitial oxygen atoms must stay far away from Cr^{3+} since no additional EPR signal was detected from different Cr^{3+} centers other than Cr^{3+} (I) and Cr^{3+}(II). The same conclusion may be drawn from our fluorescence results. However, in some poor quality samples, we did observe additional strong emission from two other Cr^{3+} sites, which are probably from clusters of a different Mg_2SiO_4 phase.[10]

In the NIR region, very strong fluorescence was detected (Fig. 5). The low temperature fluorescence consists of

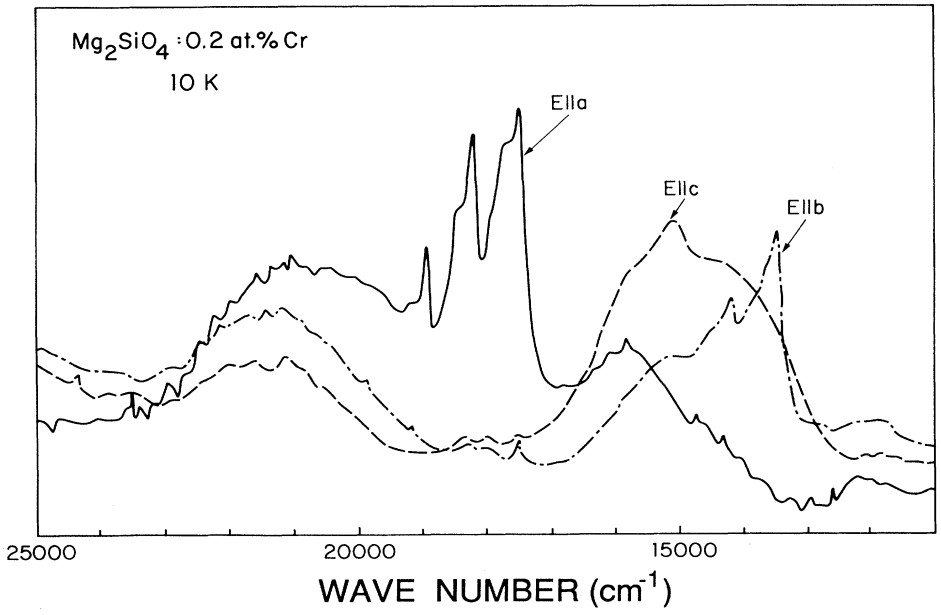

FIG. 6. The polarized absorption spectra of Mg_2SiO_4:0.2 at.% Cr in the visible region at 10 K.

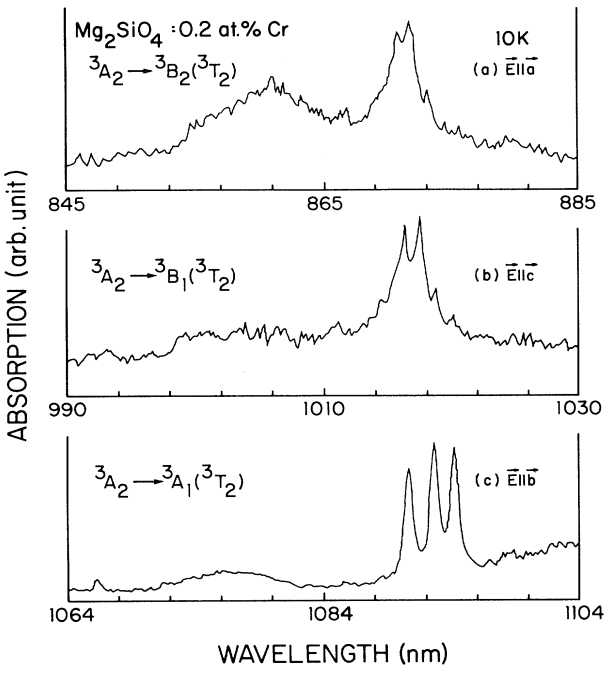

FIG. 7. The polarized absorption spectra ($^3A_2 \rightarrow {}^3T_2$) of Cr^{4+} in forsterite Mg_2SiO_4:0.2 at.% Cr in the near infrared at 10 K. (a) $E\|a$, $^3A_2 \rightarrow {}^3B_2(^3T_2)$; (b) $E\|c$, $^3A_2 \rightarrow {}^3B_1(^3T_2)$; (c) $E\|b$, $^3A_2 \rightarrow {}^3A_1(^3T_2)$.

three peaks at 1094.5 nm (9137 cm^{-1}), 1092.8 nm (9151 cm^{-1}), and 1090.6 nm (9169 cm^{-1}). The relative intensities of the fluorescence at different temperatures are shown in the inset of the figure. It can be seen that the relative intensities of the three peaks obey the Boltzman thermal distribution rule. We assigned this spectra to the $^3A_1(^3T_2) \rightarrow {}^3A_2$ transition of Cr^{4+} ions, which, as noted before, replace Si in the tetrahedral sites. The lifetime of this emission is 30 μs at 10 K and 3 μs at room temperature. The spectrum also contains a series of phonon satellites at longer wavelengths. With increasing temperature, the spectrum broadens, merging with the phonon sideband and in time overlaps the emission of Cr^{3+}, as reported in the literature.[5,6,9]

No spectral features from Cr^{2+} were observed and its presence in these samples can be ruled out.

C. Absorption

Polarized absorption spectra were measured at 10 K using the bulk samples. The results in the visible are presented in Fig. 6. The absorption spectra of Cr^{4+} in the NIR are shown in Fig. 7, and consist of transitions from the $^3A_2$ ground state to the three orthorhombic components, $^3A_1$, $^3B_1$, and $^3B_2$, of the $^3T_2$ state. Due to the overlapping spectra from Cr^{3+} (I), Cr^{3+}(II), and Cr^{4+} in the visible, it is difficult to make a convincing assignment for all the absorption peaks in Fig. 6 at this stage. Fortunately, it was found that the energy transfer from Cr^{3+}(I) to Cr^{3+}(II) and from both Cr^{3+} sites to Cr^{4+} was negligible, and was not very efficient even at room temperature. Therefore, site-selective excitation can be used to separate the overlapping spectra.

D. Site-selective excitation spectra

In the site-selective excitation measurement, the detection spectrometers were set to the fluorescence peaks of the corresponding ionic sites, that is, 14 437 cm^{-1} (692.7 nm) for Cr^{3+}(I), 11 600 cm^{-1} (862.1 nm) for Cr^{3+}(II), and 9137 cm^{-1} (1094.5 nm) for Cr^{4+}, respectively, while the source was scanned through the visible. The data were

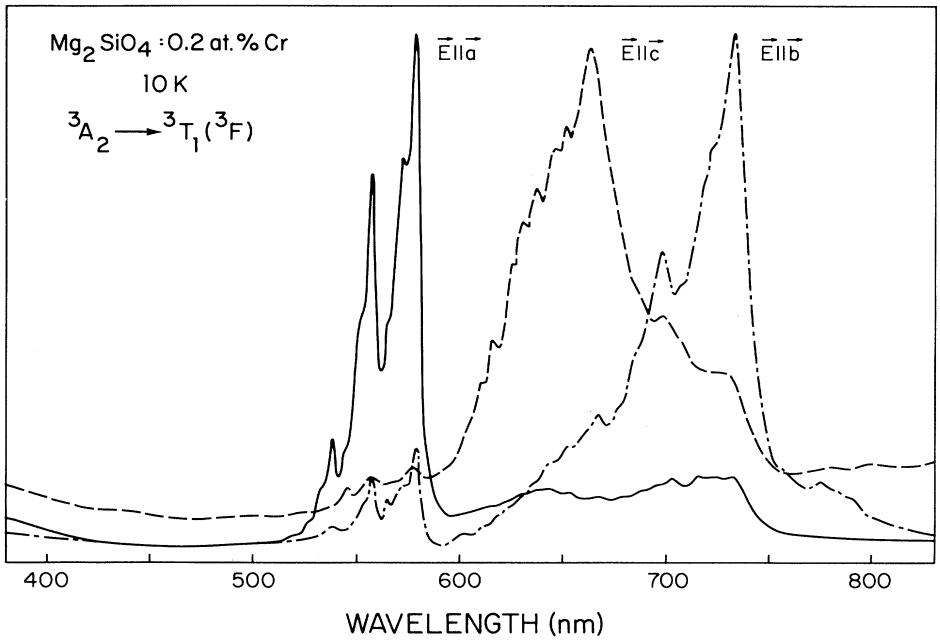

FIG. 8. The site-selective excitation spectra of Cr^{4+} in forsterite Mg_2SiO_4:0.2 at.% Cr at 10 K. The monitored wavelength is 1094.2 nm.

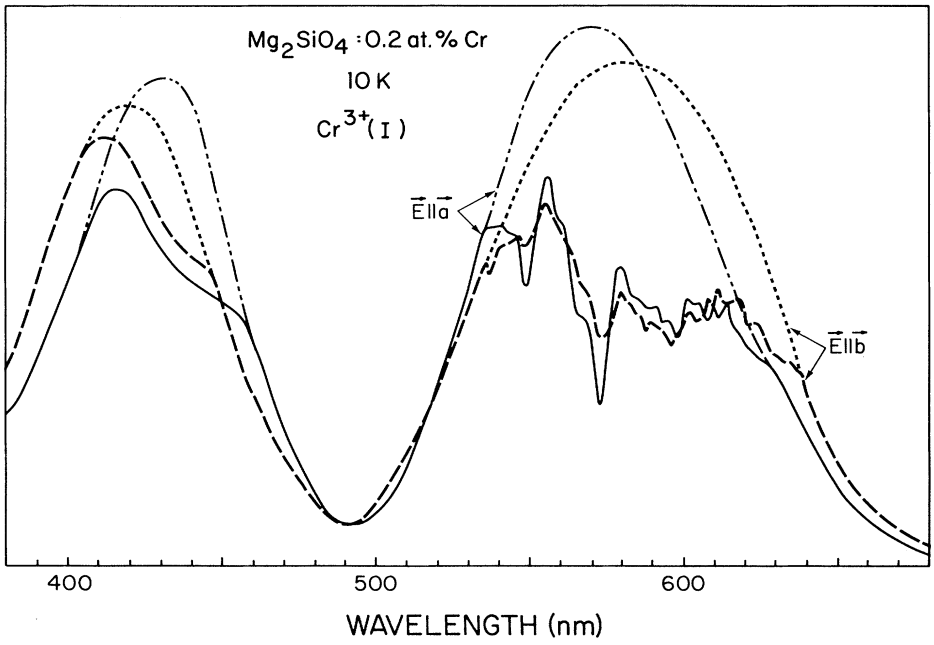

FIG. 9. The site-selective excitation spectra of Cr^{3+}(I) in forsterite at 10 K. The monitored wave number is 14437 cm^{-1}. The dot-dot-dashed lines are the corrected profiles.

stored and normalized for spectral response of the lamp and the monochromater. In the limit of slow energy transfer at 10 K, each excitation spectrum is analogous to the absorption of each ionic site.

The polarized site-selective excitation spectra of Cr^{4+} are shown in Fig. 8, and demonstrate highly anisotropic behavior. This result confirms that the dominant absorption peaks in the overall absorption of Fig. 6 are from Cr^{4+} ions. The three groups of absorption bands in the three polarizations assigned to the transition from the $^3A_2$ ground state to the three components, $^3A_2$, $^3B_1$, and $^3B_2$, of the $^3T_1$ excited state.

The site-selective excitation spectra for Cr^{3+}(I) and Cr^{3+}(II) are shown in Figs. 9 and 10, respectively. The

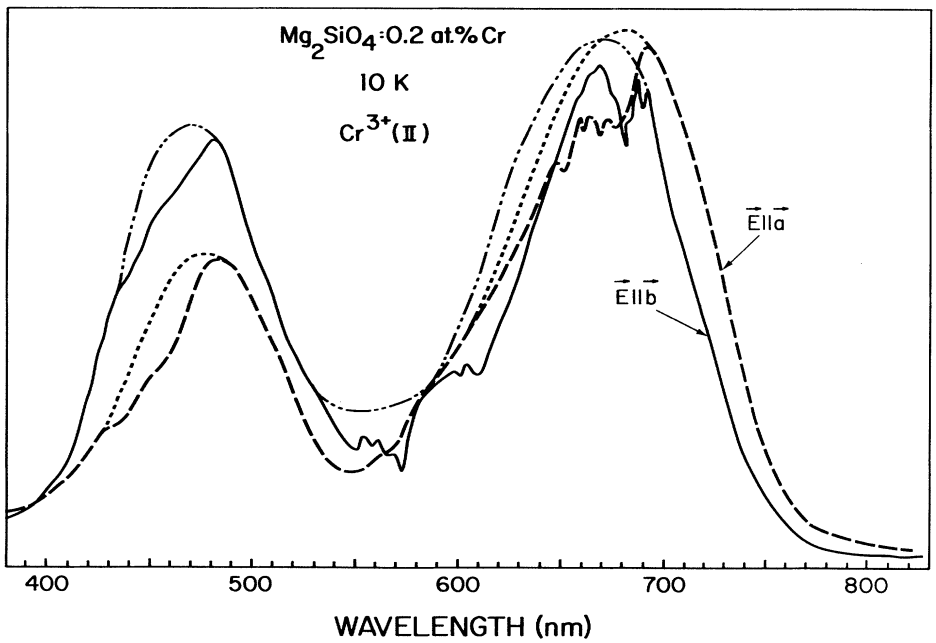

FIG. 10. The site-selective excitation spectra of Cr^{3+}(II) in forsterite at 10 K. The monitored wave number is 11600 cm^{-1}. The dot-dot-dashed lines are the corrected profiles.

spectra shows additional structure which results from absorption of Cr^{4+}.

In general, the excitation spectrum of a certain optical activator will be modulated by the absorption of other optical centers which are present. The site-selected fluorescence signal is proportional to

$$I(\lambda)=KA(\lambda)L_{\text{eff}}(\lambda)=KA(\lambda)L(\lambda)[1-B(\lambda)] . \quad (1)$$

Due to the absorbance, $B(\lambda)$, of all other optical centers, the effective incident lamp power, $L_{\text{eff}}(\lambda)$, seen by the impurity ions will not equal to the original spectral profile of the lamp, $L(\lambda)$. After normalized by $L(\lambda)$, the excitation spectrum will include the absorption of other centers present.

Taking into account of the absorption contribution to $B(\lambda)$ from Cr^{4+} and Cr^{3+}(II) or Cr^{3+}(I), then the absorption spectra from Cr^{3+}(I) and Cr^{3+}(II) can be deconvoluted, as shown by dot-dot-dashed lines in Figs. 9 and 10. Through this procedure, it can be seen that the absorption bands from Cr^{3+} in octahedral sites are normal and similar to the results of ruby or alexandrite.

IV. DISCUSSION

The experimental data indicate that the dominant absorption in the chromium-activated forsterite samples originated from Cr^{4+} ions in tetrahedral sites. In general, ions in a tetrahedron can have much higher transition probability than ions in an octahedron, since the former has no inversion symmetry.[13] On the other hand, the large anisotropies and field splittings observed for both Cr^{3+} and Cr^{4+} indicate large distortions in the polyhedrons, requiring closer examination.

A. Zero-field splitting of Cr^{3+}(I)

The field parameters for Cr^{3+} can be derived under the cubic field approximation. Using the average energies (centroid) of the absorption bands, we find, for Cr^{3+}(I), $Dq=1730\ cm^{-1}$, $B=590\ cm^{-1}$, $C=3320\ cm^{-1}$, and $C/B=5.2$; and for Cr^{3+}(II), $Dq=1490\ cm^{-1}$, $B=620\ cm^{-1}$, $C=2700\ cm^{-1}$, and $C/B=4.4$ (see Table I).

However, in forsterite all the octahedra are extremely distorted and no longer cubic. They may be approximated by a lower C_{3v} or D_{4h} symmetry.[12] Macfarlane[14] has taken the cubic field as the zeroth-order term and calculated zero-field splitting of t_2^3 in trigonally and tetragonally distorted octahedral symmetry. For Cr^{3+} (I) and tetragonal distortion, taking $\Delta(^2E)=200\ cm^{-1}$ and $d(^4A_2)=2.2\ cm^{-1}$, it was determined that the tetragonal field parameters are $\delta=10\,500\ cm^{-1}$ and $\mu=28\,600\ cm^{-1}$. For trigonal symmetry, the trigonal field parameters, v and v', were found to be $-4720\ cm^{-1}$ and $4730\ cm^{-1}$, respectively. In both cases the parameters yield values which are comparable or much higher than the Dq value; thus the uniaxial field components are too large to be taken as perturbation, and the distorted octahedron can not be approximated by any uniaxial symmetry. Such large zero-field splittings were also found in some halogeno-pentaammine-chromium (III) salts,[15,16] and current field theories have not addressed these problems. Schmidtke *et al.*[15] pointed out that complete ligand field calculation for Cr^{3+} predicted a maximal level splittings of $0.3\ cm^{-1}$ for $^4A_2$ and $50\ cm^{-1}$ for ^2E_g. The results do not change very much if various improvements are implemented. It has been suggested[15,16] that nonspherical contributions to electronic repulsion integrals may be responsible for the large splittings. The corresponding perturbation expression for the ^2E splitting is as follows:[15,16]

$$\Delta E=2\tau^2(1-\tau^2)(3B+C) . \quad (2)$$

Here τ is an effective orbital expansion parameter and B and C are the usual Racah coefficients. For Cr^{3+}(I), it was found $\tau=99\%$. Therefore, a small anisotropy in the electron repulsion energy can give a large splitting. Unfortunately, the anisotropy of the electron repulsion potential has no effect on the spin-orbit splitting of the $^4A_2$ ground state.[15]

B. The energy diagram of Cr^{4+} in orthorhombic field

In most of the previous cases studied, $3d^2$ ions, such as V^{3+} and Ti^{2+}, are situated in octahedral sites. In the forsterite case, Cr^{4+} ions replace Si and offer an unique example which demonstrates tetrahedral spectral characteristics.

From field theory, the energy diagram of $3d^2$ ions in a tetrahedron is similar to that of $3d^8$ (such as Ni^{2+}) in an octahedron. The Tanabe-Sugano diagram of $3d^2$ in a tetrahedron is shown in Fig. 11. In a tetrahedral field,

TABLE I. The energy-level positions and field parameters of the Cr^{3+}(I) and Cr^{3+}(II) ions in forsterite.

			Cr^{3+}(I)				
$^4A_2$	$^4T_2$	^2E	$^2T_1$	$^4T_1$	Dq	B	C
0	17 100	14 437.9		23 900			
			15 380[a]		1730	590	3320
2.2	17 500	14 637.9		23 200			
			Cr^{3+}(II)				
	14 800			21 100			
0		13 500			1490	620	2700
	14 900			20 800			

[a]From Ref. 5 (OSA Proceeding).

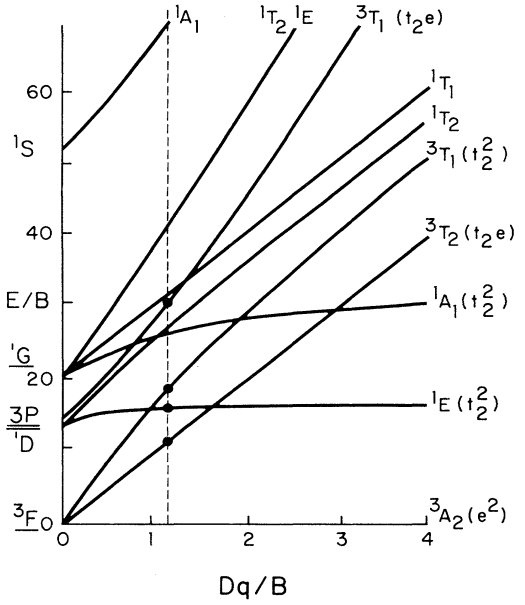

FIG. 11. Tanabe-Sugano energy level diagram of $Cr^{4+}(3d^2)$ in a tetrahedral field.

TABLE II. The energy levels of Cr^{4+} ions in forsterite, cm^{-1} (nm).

Tetrahedral	Orthorhombic	Spin-orbital coupling
$^3A_2$, 0	$^3A_2$, 0	$^3A_2 \cong 0$
		B_1 9139(1094)
	$^3A_1$, 9150	B_2 9152(1093)
		A_2 9169(1091)
		A_2 9812(1019)
$^3T_2$, 10 140	$^3B_1$, 9820	A_1 9824(1018)
		B_2 9836(1017)
		B_1 11 455(873)
	$^3B_2$, 11 470	A_1 11 472(872)
		A_2 11 489(871)
		A_1 13 684(733)
	$^3A_2$, 13 850	B_2 13 812(724)
		B_1 14 045(712)
		B_2 15 050(665)
$^3T_1$, 15 610	$^3B_1$, 15 300	A_1 15 340(652)
		A_2 15 500(645)
		A_2 17 470(572)
	$^3B_2$, 17 670	A_1 17 680(567)
		B_1 17 857(560)
^1E, 15 875[a]		
$^3T_1(^3P)$, 26 810[a]		
$^1T_1$, 28 735[a]		

[a]From Ref. 5 (OSA Proceeding).

the ^3F ground state of Cr^{4+} free ions splits into $^3A_2(e^2)$, $^3T_2(et_2)$, and $^3T_1(t_2^2)$ with $^3A_2$ as the ground state. One of the excited states of the free ions, ^3P, transforms into $^3T_1(^3P)$. The electric dipole operator transforms as T_2 so that $^3A_2 \rightarrow {}^3T_1$ transitions are allowed, but $^3A_2 \rightarrow {}^3T_2$ is forbidden. The latter become allowed in forsterite since the tetrahedron contains an orthorhombic distortion. The distortion reduces the symmetry of the tetrahedron from T_d to C_s.[6] For simplicity we took a C_{2v} approximation for it below.

The excitation spectra in Fig. 8 and the dominant absorption bands in Fig. 7 correspond to the transition $^3A_2 \rightarrow {}^3T_1$. Under a C_{2v}-orthorhombic field, $^3T_1$ splits into $^3A_2$, $^3B_1$, and $^3B_2$, absorption appearing in polarizations; $E \| c$, b, and a, respectively. Under spin-orbit interaction, the spin-triplet degeneracy of each orthorhombic field component is further split into three spin singlets. For example, $^3A_2$ becomes A_1, B_1, and B_2; $^3B_1$: A_1, A_2, and B_2; $^3B_2$: A_2, A_1, and B_1.

It can be seen from Figs. 7 and 8 that the spectrum in each polarization consists of three groups of absorption bands, and each band consists of three peaks. For example, the strongest absorption in $E \| a$ polarization has three peaks at 572 (17 470), 567 (17 680) and 560 nm (17 857 cm^{-1}); they are the zero-phonon transitions from the $^3A_2$ state to the spinors, A_2, A_1, and B_1 of $^3B_2(^3T_1)$. The other two bands are the first and second orders phonon sidebands of the zero-phonon transitions. This is the same assignment made by Rager *et al.*,[13] although they misassigned the absorption of Cr^{4+} to Cr^{3+}. The average phonon energy was found to be 750 cm^{-1} which is likely a localized stretching mode of the tetrahedron, as this frequency is not a normal mode of forsterite.[17] Comparing the total integrated intensity to that of the zero-phonon lines, the Huang-Rhys factor is found to be $S = 1.0$, corresponding to intermediate coupling for the $^3T_1$ state.

The spectra in other polarizations have similar splittings and phonon sidebands, but are generally not resolved as well as the above example. The energy-level data are collected in Table II. The average positions of the $^3A_2$, $^3B_1$, and $^3B_2$ states are at 13 850, 15 300, and 17 480 cm^{-1}.

The $^3T_2$ state splits into $^3A_1$, $^3B_1$, and $^3B_2$ components in a C_{2v} field. The three components are located on average at 9150, 9820, and 11 520 cm^{-1}, respectively; further splittings are produced by spin-orbit coupling resulting in nine spinors (Table II). As in the case of the $^3T_1$ state, the zero-phonon lines of each orthorhombic field component are also accompanied by phonon satellites in both absorption (Fig. 9) and fluorescence (for $^3A_1$, see Fig. 5). The Huang-Rhys factor of the $^3A_1$ state was found to be $S(^3A_1) = 0.7$.

The average positions of the $^3T_1$ and $^3T_2$ states are at 10 160 and 15 610 cm^{-1}, respectively. With the aid of the spectra of Petricevic *et al.*,[5] the cubic field parameters for Cr^{4+} are determined to be $Dq = 1010$ cm^{-1}, $B = 860$ cm^{-1}, and $C = 4220$ cm^{-1}, $C/B = 5.0$ and $Dq/B = 1.2$. Again, due to large distortions of the tetrahedra, the cubic field approximation is not sufficient to describe the electronic structure of Cr^{4+}, and orthorhombic field splittings have to be considered.

Ferguson *et al.*[18] have discussed the electronic energy level structure of Ni^{2+} in MgF_2, where $Ni^{2+}(3d^8)$ is in an orthorhombic-distorted octahedron. $Cr^{4+}(3d^2)$ in an tetrahedron may have a similar energy level picture. In terms of the pseudoangular momentum operators, L_x,

TABLE III. The spinors' eigenvalues of the $^3T_2$ state of Cr^{4+} in forsterite.

$^3A_1(^3T_2)$	$E(B_1)=-\Delta/3-\Gamma-A-(\lambda-A)^2/(\Delta+\Delta)$
	$E(B_2)=-\Delta/3-\Gamma-\lambda^2/2\Gamma$
	$E(A_2)=-\Delta/3-\Gamma-A'-(\lambda-A+A')^2/(2\Gamma-A)$
$^3B_1(^3T_2)$	$E(A_2)=-\Delta/3+\Gamma-A-A'+(\lambda-A+A')^2/(2\Gamma-A)$
	$E(A_1)=-\Delta/3+\Gamma+\lambda^2/(\Delta-\Gamma)$
	$E(B_2)=-\Delta/3+\Gamma+\lambda^2/2\Gamma$
$^3B_2(^3T_2)$	$E(B_1)=2\Delta/3-A+(\lambda-A)^2/(\Delta+\Gamma)$
	$E(A_1)=2\Delta/3-\lambda^2/(\Delta-\Gamma)$
	$E(A_2)=2\Delta/3-A'+(\lambda-A+A')^2/(\Delta-\Gamma+A)$

L_y, and L_z, the effective Hamiltonian in an orthorhombic field can be written[18]

$$H=-\Delta(L_z^2-\tfrac{2}{3}-\Gamma(L_x^2-L_y^2)+(\lambda_x S_x L_x+\lambda_y S_y L_y+\lambda_z S_z L_z)+H_{\text{cubic}'} \quad (3)$$

and

$$H_{\text{cubic}}=A[(S-L)^2-2(S_{x'}^2L_{x'}^2+S_{y'}^2L_{y'}^2+S_{z'}^2L_{z'}^2)+1]+A'[-(\mathbf{S}\cdot\mathbf{L})^2+1] .$$

The first term represents the axial field and the second term is the orthorhombic field. The third term is the spin-orbit interaction; xyz and $x'y'z'$ refer to the crystallographic and Cr^{4+}-tetrahedral coordinates, respectively.

Neglecting configuration interaction, and omitting the spin-orbit coupling at this stage, the basis set for the $^3T_2$ wave function in a C_{2v} symmetric field is chosen as

$$\psi(^3A_1)=\psi(^3T_2z'^2) ,$$

$$\psi(^3B_1)=\psi(^3T_2z'x') , \quad \psi(^3B_2)=\psi(^3T_2z'y') , \quad (4)$$

with energies $-\Delta/3+\Gamma$, $-\Delta/3-\Gamma$, and $2\Delta/3$, respectively. This leads to $\Delta=1985\ \text{cm}^{-1}$ and $\Gamma=335\ \text{cm}^{-1}$.

In the presence of spin-orbit coupling, the components of the $^3A_1$ state may be expressed in terms of the three $M_s(\pm1,0)$ wave functions as follows:

$$\psi(^3A_1B_2)=(1/\sqrt{2})[-\psi(^3A_11)+\psi(^3A_1-1)] ,$$

$$\psi(^3A_1B_1)=(i/\sqrt{2})[\psi^3A_11)+\psi(^3A_1-1)] , \quad (5)$$

$$\psi(^3A_1A_2)=\psi(^3A_10) .$$

In a similar way, we can construct two A_1 functions from $\psi(^3B_1)$ and $\psi(^3B_2)$, three A_2 functions from $\psi(^3A_1)$, $\psi(^3B_1)$, and $\psi(^3B_2)$, two B_1 functions from $\psi(^3A_1)$ and $\psi(^3B_2)$, and finally two B_2 functions from $\psi(^3A_1)$ and $\psi(^3B_1)$.

In the limit of $\Delta\gg\Gamma>\lambda, A, A'$, the eigenvalues of the corresponding eigenstates can be found from the secular matrix of the Hamilitonian. The results are listed in Table III. An experimental fit leads to $\lambda=116\ \text{cm}^{-1}$, $A=30\ \text{cm}^{-1}$, and $A'=5\ \text{cm}^{-1}$. A similar analysis can be applied to the $^3T_1(^3F)$ state.

The spin-orbit splitting of the $^3A_2$ ground state of Cr^{4+} must be very small in forsterite. By means of second-order perturbation theory, the zero-field-splitting parameters, D and E, of the $^3A_2$ ground state can be found to be related to Δ and Γ as follows:[18]

$$D=\Delta(\xi/W)^2 \text{ and } E=\Gamma(\xi/W)^2 . \quad (6)$$

Here $\xi=2S\lambda$, is the one-electron spin-orbit coupling parameter in the cubic field approximation. For Cr^{4+} free ions, $\lambda_0=164\ \text{cm}^{-1}$ and $\xi_0=328\ \text{cm}^{-1}$.[19] We take $\xi=200\ \text{cm}^{-1}$, 80% of the free-ionic value. W is the energy separation between $^3T_2$ and $^3A_2$, which is $10\,140\ \text{cm}^{-1}$. Adopting $\Delta=1985\ \text{cm}^{-1}$ and $\Gamma=335\ \text{cm}^{-1}$, we find that $D=0.77\ \text{cm}^{-1}$ and $E=0.13\ \text{cm}^{-1}$. Considering the linewidth, 8 cm^{-1}, of the $B_1(^3A_1)$ to $^3A_2$ transition at 10 K, such small splittings cannot be resolved in our experiment. This analysis further confirms the conclusion that the three sharp peaks of the transition between the $^3A_2$ and $^3A_1(^3T_2)$ states [Figs. 5 and 7(c)] originates from the excited state splitting.

V. CONCLUSION

Chromium-doped forsterite samples show fluorescence emission from both Cr^{3+} and Cr^{4+} ions. Cr^{3+} ions are found in two types of octahedral sites: Mg(I) with inversion symmetry and Mg(II) with mirror symmetry, resulting in high and low field sites, respectively. Cr^{4+} replaces Si at tetrahedral sites. The dominant absorption bands in the visible is identified as the $^3A_2\rightarrow{}^3T_1$ transition, while the emission in the NIR results from the $^3A_1(^3T_2)$ to the $^3A_2$ ground state transition. We discuss the Cr^{4+} spectra in terms of an orthorhombic-distorted tetrahedral field.

ACKNOWLEDGMENTS

We are grateful to Dr. E. Strauss, S. Jacobsen, and B. Tissue for helpful discussion, and to L. Lu for growing the fiber samples. This work was supported by the Department of Energy (DOE) under Grant No. DE-FG09-87ER45291.

[1]J. C. Walling, O. G. Peterson, H. P. Jenssen, R. C. Morris, and E. W. O'Dell, IEEE J. Quantum Electron. **QE-16**, 1302 (1980).

[2]B. Struve, G. Huber, V. V. Laptev, I. A. Shcherbakov, and E. V. Zharikov, Appl. Phys. B **30**, 117 (1983).

[3]P. F. Moulton, J. Opt. Soc. Am. **B3**, 125 (1986).

[4]V. Petricevic, S. K. Gayen, R. R. Alfano, K. Yamagishi, H. Anzai, and Y. Yamaguchi, Appl. Phys. Lett. **52**, 1040 (1988).

[5]V. Petricevic, S. K. Gayen, and R. R. Alfano, Optics Lett. **14**, 612 (1989); Appl. Phys. Lett. **53**, 2590 (1988); *OSA Proceeding on Tunable Solid State Lasers,* edited by M. L. Shand and H. P. Jenssen (Optical Society of America, Woodbury, NY, 1989), Vol. 5, p. 77.

[6]H. R. Verdun, L. M. Thomas, D. M. Andrauskas, T. McCollum, and A. Pinto, Appl. Phys. Lett. **53**, 2593 (1988); *OSA Proceeding on Tunable Solid State Lasers,* Ref. 5, p. 85.

[7]Z. Goldschmidt, W. Low and M. Foguel, Phys. Lett. **19**, 17 (1965); B. Champaynon and E. Duval, J. Phys. (Paris) **38** L299 (1977).

[8]S. M. Jacobsen, W. E. Smith, C. Reber, and H. V. Gudel, J. Chem. Phys. **84**, 5205 (1986); S. M. Jacobsen, H. V. Gudel, and C. A. Daul, Chem. Phys. Lett. **158**, 77 (1989); J. Am. Chem. Soc. **110**, 7610 (1988); S. M. Jacobsen and H. V. Gudel, J. Lumin. **43**, 125 (1989).

[9]R. Moncorge, D. J. Simkin, G. Cormier and J. A. Capobianco, in *OSA Proceeding on Tunable Solid State Lasers,* Ref. 5, p. 93.

[10]Weiyi Jia, Lizhu Lu, B. Tissue, and W. M. Yen, J. Crystal Growth (to be published).

[11]J. D. Birle, G. V. Gibbs, P. B. Moore, and J. V. Smith, Amer. Mineral. **53**, 807 (1968).

[12]H. Rager and G. Weiser, Bull. Mineral. **104**, 603 (1981).

[13]B. Henderson and G. F. Imbusch, *Optical Spectroscopy of Inorganic Solid* (Clarendon, Oxford, 1989), p. 77.

[14]R. M. Macfarlane, J. Chem. Phys. **47**, 2066 (1967).

[15]H. H. Schmidtke, H. Adamsky, and T. Schonherr, Bull. Chem. Soc. Jpn. **61**, 59 (1988)

[16]H. Riesen, E. Krousz, and L. Dubicki, J. Lumin. **44**, 79 (1989).

[17]K. Iishi, Amer. Mineral. **63**, 1198 (1978).

[18]J. Ferguson, H. J. Guggenheim, H. Kamimuru, and Y. Tanabe, J. Chem. Phys. **42**, 775 (1965).

[19]A. Abragam and B. Bleaney, *Electron Paramagnetic Resonance of Transition Ions* (Oxford University Press, Oxford, 1970), p. 399.